LA-UR-12-24873
Approved for public release; distribution is unlimited.

Title: Tuning the DARHT Long-Pulse Linear Induction Accelerator

Author(s): Ekdahl, Carl A. Jr.

Intended for: 19th International Conference on High-Power Particle Beams, 2012-09-30 (Karlsruhe, ---, Germany)

Tuning the DARHT Long-Pulse Linear Induction Accelerator

Carl Ekdahl
Los Alamos National laboratory
Los Alamos, NM, USA

***Abstract*—Flash radiography of large hydrodynamic experiments driven by high explosives is a well-known diagnostic technique in use at many laboratories. The Dual-Axis Radiography for Hydrodynamic Testing (DARHT) facility at Los Alamos produces flash radiographs of large hydrodynamic experiments. Two linear induction accelerators (LIAs) make the bremsstrahlung radiographic source spots for orthogonal views of each test. The 2-kA, 20-MeV Axis-I LIA creates a single 60-ns radiography pulse. The 1.7-kA, 16.5-MeV Axis-II LIA creates up to four radiography pulses by kicking them out of a longer pulse that has a 1.6-μs flattop.**

The DARHT LIAs use solenoidal focusing for transport of the beam through the accelerators. The long-pulse Axis-II LIA has 74 accelerating cells, and uses 91 solenoids and 80 pairs of dipoles for focusing, transport, and steering the beam. The setting the currents of these 251 magnets is called tuning the accelerator. The design of the focusing tune is computationally intensive. Focusing tune design methods, simulations, and validation are the main topics of this article.

Keywords—linear induction accelerator; beam transport; beam focusing; beam dynamics

I. INTRODUCTION

Flash radiography of large hydrodynamic experiments driven by high explosives is a well-known diagnostic technique in use at many laboratories. At Los Alamos, the Dual-Axis Radiography for Hydrodynamic Testing (DARHT) facility produces multiple flash radiographs from different directions of hydrodynamic experiments. Two linear induction accelerators (LIAs) make the bremsstrahlung radiographic source spots for orthogonal views of each test. The 2-kA, 20-MeV Axis-I LIA creates a single 60-ns radiography pulse. The 1.7-kA, 16.5-MeV Axis-II LIA creates up to four radiography pulses by kicking them out of a longer pulse that has a 1.6-μs flattop. The Axis-II injector, LIA, kicker, and downstream transport (DST) to the bremsstrahlung converter are described in [1-5].

DARHT Axis-II uses solenoids for focusing the beam and dipole pairs for steering. Each cell incorporates a solenoid and a co-located pair of dipoles. Including all magnets in between blocks of cells, in the diode anode region, and elsewhere, there are 91 solenoids and 80 pairs of dipoles. Adjusting the magnetic focusing and steering magnets to optimize the electron-beam transport through an LIA is often called "tuning." Thus, a total of 251 individual magnets must be set to tune the Axis-II injector and LIA.

Tuning the Axis-II LIA is done in two stages. First, the solenoidal focusing magnets are set to values designed to provide a matched beam with little or no envelope oscillations, and little or no beam-breakup (BBU) instability growth. Then, steering elements are adjusted to minimize the motion of the centroid of a well-centered beam at the LIA exit. As in all high-current LIAs, the focusing field is designed to be as close to that of the ideal continuous solenoid as physically possible. In ideal continuous solenoidal transport a smoothly varying beam size can easily be found for which radial forces balance, and the beam is said to be "matched" to the focusing field. A "mismatched" beam exhibits unwanted oscillations in size, which are a source of free energy that contributes to emittance growth. This is undesirable, because in the absence of beam-target effects, the radiographic spot size is proportional to the emittance. The tunes for Axis-II incorporate measures to mitigate BBU instability, image displacement instability (IDI), corkscrew motion (beam sweep), and emittance growth.

Section II covers the general approach to of design of focusing solenoid tunes for the DARHT Axis-II LIA. Section III presents some evidence for the validity of the simulations used for design of the focusing tune. In Section IV we discuss simulations intended to provide insight into the vulnerability of our tunes to the growth of emittance in the LIA. We provide a brief discussion of the methods we use to tune the steering dipoles in Section V; details are readily available in [4].

II. TUNE DESIGN SIMULATIONS

Designing a focusing tune for DARHT relies heavily on a number of beam dynamics simulation codes. The primary tools are codes that solve the second-order differential equations for the beam envelope [6, 7, 8]. A code that we use extensively for tuning both DARHT LIAs is the XTR envelope code written by Paul Allison [9,10]. XTR solves for the beam envelope radius and its first spatial derivative, the envelope divergence, as functions of position. The initial parameters required by XTR at the beginning of the integration are the beam kinetic energy, the beam current, the

Research supported by the U. S. Department of Energy and the National Nuclear Security Administration under contract DE-AC52-06NA25396.

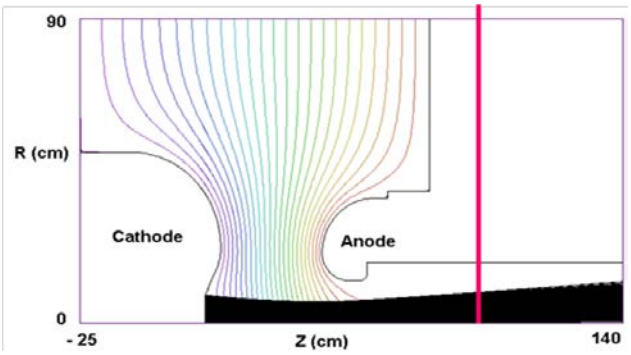

Figure 1: TRAK simulation of 1.7-kA space-charge limited current produced by the hot dispenser cathode in the Axis-II diode biased to 2.2 MV. The initial conditions for the envelope codes obtained at the position of the vertical red line (z=100cm) were r0=8.8 cm and r0'=24.7mr. The normalized emittance at that location was 178 π-mm-mr from the TRAK simulation.

beam emittance, and the two initial conditions: radius and divergence. The initial beam kinetic energy is that acquired by acceleration through the diode AK gap. Also required is a model of the accelerator which includes locations and values for accelerating gaps, locations and energizing currents for focusing solenoids, and beam tube and aperture sizes. Acceleration is calculated from a thin lens model of the potential in the gaps. The solenoidal focusing field in XTR is calculated from solenoid models that have parameters fit to experimental measurements.

Another envelope code that we use is LAMDA, which has the capability of modeling the time-resolved transport of a realistic beam-pulse waveform [11,12]. LAMDA does this by subdividing the beam pulse into slices, which are each treated as time independent, and disconnected, envelopes; a technique has been shown to agree with complex experiments [13]. Both XTR and LAMDA have higher order corrections to the simple envelope equations derived in ref. [6, 7, 8] to account for space-charge potential depression in the beam and the beam diamagnetism. LAMDA and XTR have been extensively

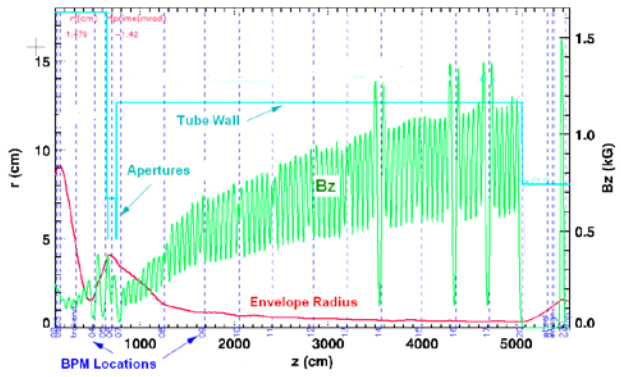

Figure 2: XTR envelope code simulation of beam transport through the injector cell block and through the BCUZ apertures into the main LIA. The solenoidal magnetic field strength on axis is denoted by the light green curve (legend on right). The red curve is the beam envelope during the 1.68-kA, 2.2-MeV flat-top of the diode pulse. Light blue lines show the beam tube, and dark blue dashed lines show the locations of BPMs.

compared with each other, and with experimental data, over the course of commissioning the DARHT LIAs. There is agreement between codes and experiment in all cases examined. The envelope codes have also been found to agree with the LSP particle-in-cell (PIC) code [14], with an LSP-based slice code [15], and with the TRAK finite-element ray-trace code [16].

Because the envelope codes are essentially second-order differential equation solvers, they require the envelope radius and divergence at the exit of the diode as initial conditions. Unlike Axis-I, we have no direct measurements of the properties of the beam as it exits the diode, so we must rely on computer simulations of the diode to provide these initial conditions. Space-charge limited diode simulations were performed in 2-D using the TRICOMP suite of codes[17, 18], which include TRAK. The results of the TRAK simulations were substantially in agreement with simulations of the same geometry and applied magnetic fields using the LSP PIC code [13]. Beam parameters obtained from these simulations are used to initialize XTR and LAMDA. The initial conditions, the space-charge limited current, and the normalized emittance were obtained from simulations with anode-cathode (A-K) voltages ranging from 100 kV to 2.8 MV, so that XTR and LAMDA could be used to predict beam behavior during the long, ~500–ns beam risetime [1,2].

Figure 1 illustrates a TRAK simulation of the DARHT Axis-II diode, showing the equipotentials and the space-charge limited electron beam at maximum current. The initial conditions for XTR and LAMDA determined from TRAK at ~80 cm downstream from the cathode surface, (Z = 100 cm) were r0=8.8 cm and r0'=24.7mr. The normalized emittance at that location was 178 -mm-mr from the TRAK simulation. Using these initial conditions, a tune was designed with XTR resulting in the predicted beam envelope shown in Fig. 2.

III. Validation of Simulations

Since the focusing tune is so heavily dependent on

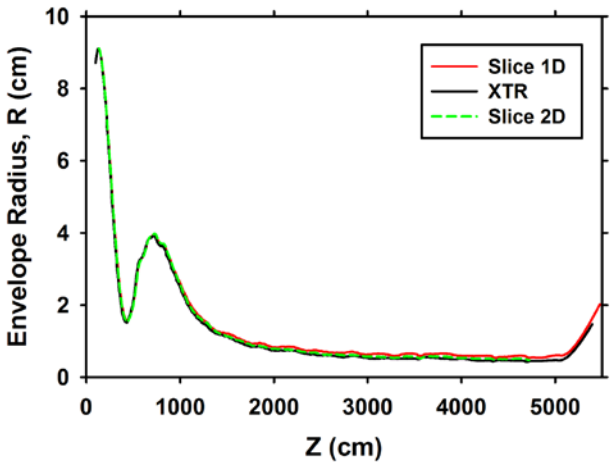

Figure 3: Comparison of two LSP-based PIC slice codes [15] with the XTR envelope code. All simulations usied the same magnetic focusing fields and initial conditions.

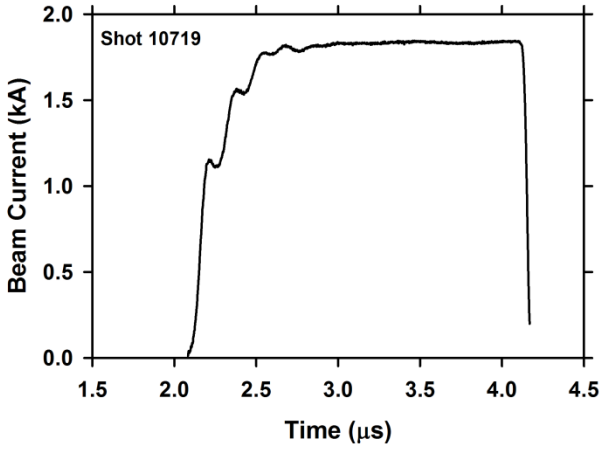

Figure 4: Measured beam current through the diode anode showing the ~500 ns risetime with 6.5-MHz LC oscillations. The pulse is sharply terminated by the crowbar switch.

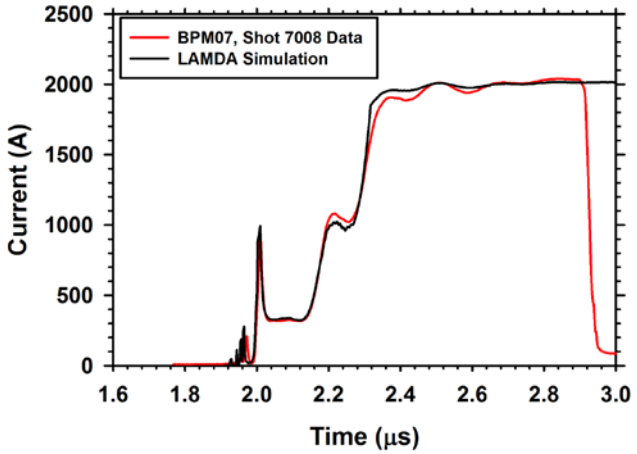

Figure 6: Current transmitted through the BCUZ (compare with diode current in Fig. 4).. The shorter pulse (shown in red) is data from shot 7008 from the first BPM beyond the BCUZ apertures. The longer pulse (shown in black) is the result of the LAMDA simulation. The LAMDA simulation used time varying initial conditions derived from TRAK simulations of the diode at AK voltages ranging from 100 kV to 2.8 MV.

simulations we have strived to challenge these in every way possible in order to gain confidence in their results. For example, we have compared the results of the envelope codes with each other [19], and also with PIC codes [15] (see Fig. 3). Although these comparisons are encouraging, especially considering the physical approximations inherent in the envelope codes, we attempt to compare with experimental data wherever possible. For example, time-resolved beam images obtained after the accelerator exit have agreed with code predictions to well within experimental error for several different configurations of the Axis-II accelerator [2, 20, 21].

We have also compared the diode simulations with experimental data. Figure 4 shows the measured beam current exiting the anode for a recent shot, illustrating the typically long risetime with LC oscillations from the large inductances and capacitances in the high-voltage feed for the diode. The pulse is terminated by a diverter switch called the "crowbar" (C/B).

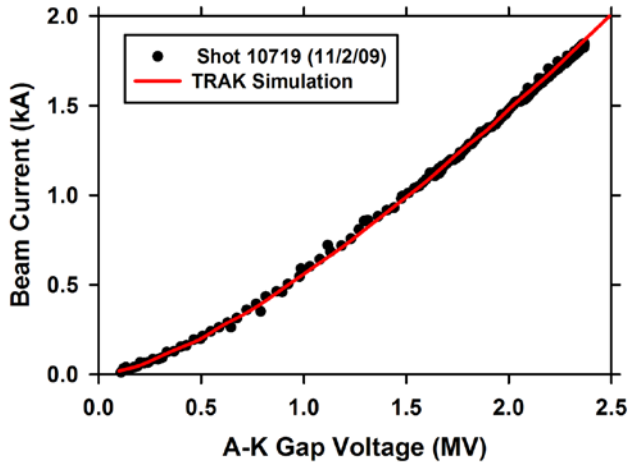

Figure 5: Diode current-voltage characteristic curve as measured experimentally compared with the curve generated from TRAK simulations. The experimental data covers the entire pulse shown in Fig. 4 for which the AK voltage was greater than 100 kV.

One experimental test of the diode simulations is to compare the measured current and voltage with the simulation results. This comparison is shown in Fig. 5, which includes all of the data for the pulse shown in Fig. 4 for which the diode AK voltage was greater than 100 kV. It includes experimental data from both the slow risetime beam head and the fast C/B initiated falltime. The agreement between simulation and experiment is within measurement uncertainty over a range of beam energy from non-relativistic to relativistic.

The envelope simulations of the beam accelerated through the injector cells have also been experimentally validated over a wide range of beam parameters. As described earlier, in lieu of experimental measurements, we rely on TRAK gun-design simulations of the diode to provide the initial conditions for the XTR or LAMDA envelope codes.

One way to experimentally confirm this procedure is to measure the current passed through the apertures shown in Fig. 2 during the off-energy beam risetime. During this time the beam has a continuously varying envelope, some of which is scraped off by the apertures. This causes a time dependent variation of the transmitted current, and to the extent that the envelope calculation using TRAK-derived initial conditions agrees with the experimental data, we have validated this approach.

Figure 6 shows such a comparison between the LAMDA envelope simulation of apertured current and the current measured just downstream of the apertures. The agreement

between theory and experiment seen in the figure lends confidence in using TRAK to establish initial conditions for the envelope codes. The agreement also demonstrates the envelope codes' ability to accurately predict the size of an obviously non-paraxial beam between the diode exit and the apertures (see Fig. 2).

IV. Emittance Growth

We used the PIC slice codes based on LSP to investigate the vulnerability of our tunes to emittance growth. One of the requirements of our tunes is that they produce a matched beam with little or no envelope oscillations during the flattop. A badly mismatched beam exhibits large envelope oscillations, sometimes called a "sausage," "m=0," or "breathing" mode. The free energy in these oscillations feeds the growth of emittance [22]. The detailed mechanism of this contribution to emittance growth is parametric amplification of electron orbits that resonate with the envelope oscillation, expelling those electrons from the beam core into a halo [23,24].

Another well-known contributor to emittance growth in solenoidal focusing systems is cumulative spherical aberration [22,25], which also over-focuses the edge of the beam, producing hollow beam profiles [26]. However, even though the cumulative spherical aberration is large in our LIA, and the resulting edge focusing is evident in PIC simulations, the resulting emittance growth is small because the beam is rapidly focused to a size much smaller than the bore of the solenoids. Essentially all of the emittance growth observed in PIC code simulations appears to come from the parametric amplification of orbits, so we emphasize matched beam envelopes in the design of our tunes.

Emittance growth was calculated using LSP PIC code simulations that model a slice of the beam as it transports through the accelerator. Two slice models have been used; Slice "1D" models a centered beam in cylindrical coordinates [15], and Slice "2D" uses Cartesian coordinates to be able to simulate the motion of the beam centroid, and fully resolve the 4-D transverse phase space.

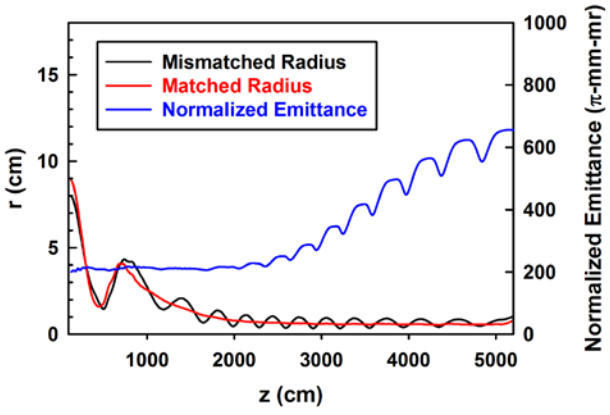

Figure 9: Equivalent envelope of a matched beam (red) compared with a badly mismatched beam (black). The emittance growth as simulated by the Slice 1D PIC code is shown in blue.

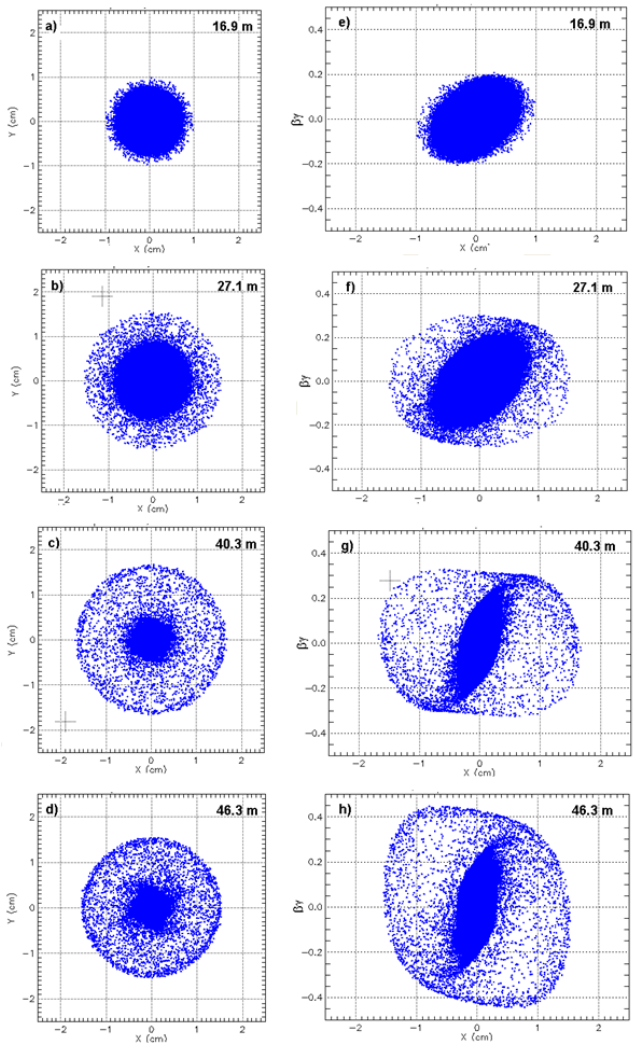

Figure 8: Left column (a, b, c, d): Configuration space (x,y) showing growth of halo as mismatched beam propagates through LIA (top to bottom). Right column (d, e, f, g): Phase space (x,px) showing resonant particle ejection into the halo, with a correspondingly larger momentum ($\beta\gamma$) contribution to emittance as the beam propagates through the LIA.

There was no calculated emittance growth in the main accelerator for a matched beam, even though there is appreciable cumulative spherical aberration in the LIA. The only growth from the initial diode emittance was ~10% increase in the injector cells, where the beam is large (Fig. 2). Moreover, no emittance growth resulted from a matched beam initially offset by as much as 1 cm. The ensuing helical motion through the solenoidal guide field does not appear to contribute to emittance growth, at least in these PIC code simulations. However, there was considerable growth when the beam was highly mismatched. Figure 7 shows the growth of emittance calculated for a significantly mismatched beam. This was accompanied by damping of the envelope oscillations as the oscillation energy was randomized. That the emittance growth is due to parametric amplification of resonant orbits producing a halo is confirmed through examination of the evolution of configuration and phase space snapshots taken from the beam slice as it transports through the LIA (Fig. 8).

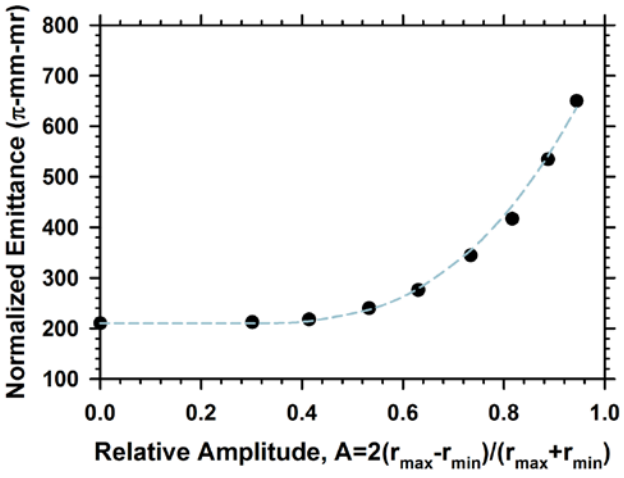

Figure 9: Emittance at the exit of the LIA (z ~ 52 m) as a function of the envelope oscillation amplitude near the beginning of observable growth (z ~ 31 m). The light blue dashed line is simply an interpolating function $\varepsilon_n = 210 + 1.4\text{E}3(A - 0.29)^{2.8}$

Fortunately, our tunes are resilient to this emittance growth mechanism; mismatches with oscillation amplitudes as large as 50% result in only ~8% growth, as shown in Fig. 9.

V. Tuning Out Beam Motion

Beam motion in the accelerator would be anathema for multi-pulse flash radiography. High frequency motion, such as from beam breakup (BBU) instability, would blur the individual spots. Low frequency motion, such as produced by pulsed power variation, would produce spot to spot differences.

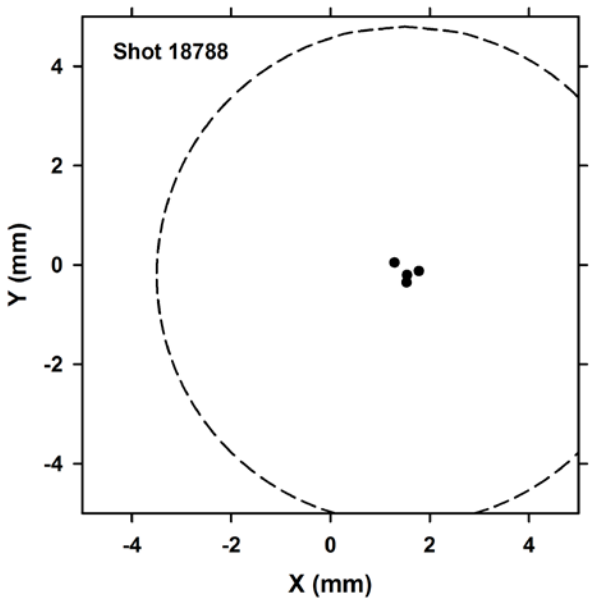

Figure 10. Position of the beam centroid at the LIA exit at the times of the four radiographs of a recent experiment (black dots). Also shown as a dashed circle is the best estimate of the beam envelope at this position.

High-frequency beam motion, with period less than the the kicked pulsewidth, would increase the radiographic source spot size, by integrating the position over the pulsewidth. The major source of high frequency motion in our LIA is the beam-breakup (BBU) instability. BBU results from beam coupling of accelerating-cell TM_{1n0} modes. Since the Axis-II cells have TM mode resonances higher than 100 MHz, large-amplitude beam breakup instability (BBU) would blur the spots of our many-ns radiographic pulses. Therefore, we have taken precautions to suppress this instability both through the design and construction of the cells and through the tuning of the accelerator focusing fields. Reference [3] details our extensive experiments to validate BBU theory on this LIA, and [4] describes recent results; the BBU peak-to-peak amplitude at the LIA exit is suppressed to less than 0.1 mm.

Low frequency beam motion, with a period greater than the kicked pulse FWHM, would result in displacement of the centers of successive radiographic source spots. Each pulse has enough energy density to erode the converter target, so displacement of early pulses in a sequence could lead to azimuthally asymmetric target material and distorted spots for later pulses. Uncorrected beam motion at the exit of the Axis-II LIA was substantial, and would have caused the radiographic source spots to meander by more than their size. The sources of this motion are asymmetric injection from the diode into the solenoidal focusing field, solenoid misalignment in the LIA, and small temporal variation in accelerating potentials. We use the steering dipoles to suppress this motion at the LIA exit to less than 1 mm over the four-pulse radiographic format; the methods we use to do this are detailed in [4]. Figure 10 shows the position of the beam centroid at the LIA exit at the times of the four radiographs of a recent experiment. The dashed circle in the figure depicts the estimated beam size for reference.

Acknowledgment

The author thanks the expert DARHT technical staff and operations crew for implementing the tunes designed with these simulations, and providing the data for validation. He also acknowledges the intellectual stimulation of a multitude of interesting discussions with numerous colleagues during the commissioning and tuning of the DARHT Axis-II LIA since first beam in 2002. Especially appreciated are technical conversations with J. Johnson, B. T. McCuistian, D. Moir, K. Nielsen, C. Rose, and M. Schulze.

References

[1] Carl Ekdahl, et al., "First beam at DARHT-II," in Proc. 2003 Part. Accel. Conf., (2003), pp. 558-562.

[2] Carl Ekdahl, et al., "Initial electron-beam results from the DARHT-II linear induction accelerator," IEEE Trans. Plasma Sci., vol. 33, (2005), pp. 892-900.

[3] Carl Ekdahl, et al., "Long-pulse beam stability experiments on the DARHT-II linear induction accelerator," IEEE Trans. Plasma Sci. , vol. 34, (2006), pp.460-466.

[4] Carl Ekdahl, et al., "Suppressing beam-centroid motion in a long-pulse linear induction accelerator," Phys. Rev. Special Topics-Accelerators and Beams, vol. 14, (2011) 120401.

[5] Martin Schulze, et al., "Commissioning the DARHT-II Accelerator Downstream Transport and Target," in Proc. 2008 Linear Accel. Conf., (2008) , pp. 427-429.

[6] E. P. Lee and R. K. Cooper, "General envelope equation for cylindrically symmetric charged-particle beams," Part. Acc. , vol. 7, (1976), pp. 83-95.

[7] M. Reiser, *Theory and design of charged particle beams*, (Wiley, New York, NY 1994).

[8] S. Humphries, Jr., *Charged particle beams*, (Wiley, New York, 1990)

[9] P. Allison, "XTR, a new beam dynamics code for DARHT," DARHT Tech Note #50, (1995), unpublished,.

[10] Thomas P. Hughes, David C. Moir, and Paul W. Allison, "Beam injector and transport calculations for ITS," in Proc. 1995 Part. Accel. Conf., (1995), pp. 1207-1209.

[11] Thomas C. Genoni, Thomas P. Hughes, and Carsten H. Thoma, "Improved envelope and centroid equations for high current beams", AIP Conf. Proc., vol. 650, (2002), p. 463.

[12] Thomas P. Hughes, et al., "LAMDA User's Manual and Reference", Voss Scientific technical report VSL-0707, April 2007.

[13] C.A. Ekdahl, "Modeling Ion-Focused Transport of Electron Beams With Simple Beam-Envelope Simulations," Sandia National Laboratory Report, SAND-0544, 1986 (National Technical Information Service DE86012739).

[14] Y. Tang, T. P. Hughes, C. A. Ekdahl, and M. E. Schulze, "Beam Clean-Up Zone Calculations for 2.5 MV, 1.4 kA Experiments on DARHT-2," in Proc. 16th International Pulsed Power Conf., (2007), pp. 1257-1260.

[15] C. Thoma, and T. P. Hughes, "A beam-slice algorithm for transport of the DARHT-2 accelerator," in Proc. 2007 Part. Accel. Conf., (2007), pp. 3411-3413.

[16] Stanley Humphries Jr., "TRAK – Charged particle tracking in electric and magnetic fields," in Computational Accelerator Physics, R. Ryne Ed., New York: American Institute of Physics, (1994), pp. 597-601.

[17] Technical information about the TriComp series of codes is available at www.fieldp.com.

[18] Stanley Humphries Jr., *Field solutions on computers*, (CRC Press Boca Raton, FL 1997) and www.fieldp.com.

[19] Carsten Thoma, Thomas P. Hughes, and Craig Miller, "Envelope and centroid equations in LAMDA and XTR codes," Voss Scientific technical report VSL-0808, March 2008.

[20] H. Bender, et al., "Quasi-anamorphic optical imaging system with tomographic reconstruction for electron beam imaging," Rev. Sci. Instrum. 78, (2007), pp.013301-1 - -13301-8.

[21] Carl Ekdahl, et al., "Commissioning the DARHT-II Scaled Accelerator," in Proc. 2007 Part. Accel. Conf., (2007) PAC07, pp. 2373-2375.

[22] M. Reiser, *Theory and design of charged particle beams*, (Wiley, New York, NY 1994) p. 467 *et seq.*

[23] T. P. Wangler, et al., "Particle-core model for transverse dynamics of beam halo," Phys. Rev. Special Topics- Accel. Beams, vol. 1, (1998), p. 084201.

[24] R. L. Guckstern, "Analytic model for halo formation in high current ion linacs," Phys. Rev. Lett., vol. 73, (1994), p. 1247.

[25] P. Loschialpo, et al., "Effects of space charge and lens aberrations in the focusing of an electron beam by a solenoid lens," J. Appl. Phys., vol. 57, (1985) pp. 10-17.

[26] S. Bernal, et al., "Edge imaging in intense beams," Phys. Rev. –STAB , vol. 5, (2002) p. 064202.